Pergamon

Tetrahedron, Vol. 52, No. 14, pp. 5161-5178, 1996

0040-4020/96 $15.00 + 0.00

S0040-4020(96)00122-6

Thermodynamic Limitations for Fullerene Formation in Flames

Christopher J. Pope and Jack B. Howard*

Department of Chemical Engineering
Massachusetts Institute of Technology
Cambridge, Massachusetts 02139

Abstract: Thermodynamic driving forces for fullerene formation in flames are considered from three different perspectives: 1) global equilibrium, 2) free energy changes for individual reactions leading to fullerene formation, and 3) relative stabilities of $C_{30}H_x$ polycyclic aromatic hydrocarbons (PAH). The ranges of conditions which promote formation of fullerenes and their precursors are determined.

INTRODUCTION

The discoverers of fullerenes suggested that these molecules may exist in sooting flames[1-4]. Early concepts of the possible interrelation of fullerenes and soot have been reviewed by Kroto et al.[5-7]. Detection of all-carbon ions with charge/mass ratios corresponding to fullerenes by Homann et al.[8,9] provided the first evidence of fullerene formation in flames. Other interesting but inconclusive evidence came from MIT[10-12]. Later, soon after the technique for producing macroscopic quantities of fullerenes by graphite vaporization via resistive heating was discovered[13] and implemented[14-16], fullerenes C_{60} and C_{70} were found in substantial quantities in sooting and near-sooting low-pressure premixed laminar flat flames[17-19]. The yield of C_{60} plus C_{70} was as much as 20% of the soot and up to 0.5% of the carbon fed in flames under certain conditions[20]. Also it was found that benzene/oxygen flames produced appreciably more fullerenes than acetylene/oxygen flames, and the molar C_{70}/C_{60} ratio varies by over an order of magnitude, with many of the flames producing more C_{70} than C_{60}.

A detailed chemical kinetic mechanism for formation of fullerenes C_{60} and C_{70} has been constructed and tested[21-23]. Fullerene formation is described as proceeding from fluoranthene ($C_{16}H_{10}$) through curved PAH intermediates of C_{5v} symmetry, i.e.: corannulene -- COR (dibenzo[ghi,mno]fluoranthene, $C_{20}H_{10}$); 1/2-bucky -- HB (pentacyclopenta[bc,ef,hi,kl,no]corannulene, $C_{30}H_{10}$); 2/3-bucky -- TB (pentabenzo[bcd,fgh,jkl,nop,rst]1/2-bucky, $C_{40}H_{10}$); 5/6-bucky -- FB (pentabenzo[bcd,fgh,jkl,nop,rst]2/3-bucky, $C_{50}H_{10}$); expanded-bucky -- XB (pentabenzo[bcd,fgh,jkl,nop,rst]5/6-bucky, $C_{60}H_{10}$). All the intermediates in the reaction mechanism (and the nomenclature used in the present work) are defined in reference 22. Much of the sequence of intermediates in the mechanism parallels the "minimum number of dangling bonds" series of species considered by Smalley[24] if all dangling bonds are capped with hydrogen atoms.

The mechanism describes C_{60} and C_{70} formation in terms of types of

reactions already known to occur in the formation of polycyclic aromatic hydrocarbons (PAH). Four classes of reactions are of importance in the fullerene formation mechanism: H-abstraction from the PAH via H-atom to form a σ-radical (Type 1); C_2H_2-addition to an aryl radical, with subsequent ring formation and H-atom loss (Type 23); cyclization of an aromatic radical to form an additional 5-membered ring (5-ring) or 6-membered ring (6-ring), with H-atom loss (Type 5-3); and intramolecular rearrangement as studied by Scott and Roelofs[25], in which two adjacent rings (a 5-ring and a 6-ring) effectively trade places, with the 5-ring becoming a 6-ring and vice versa, with a concurrent H-shift (Type 6). (Detailed discussion of the reaction types is found in reference 22.) In the mechanism, fullerene formation is seen as a subset of the molecular weight growth processes which also lead to planar PAH and soot. However, fullerenes are neither considered to be soot nuclei[1-4] nor, conversely, as dependent upon soot for their formation[8,26,27], although some data are consistent with the notion that, like planar PAH, fullerenes do stick to soot particles[28]. Preliminary tests of kinetic plausibility[22,23] showed the mechanism to produce C_{60} and C_{70} in times representative of those available for fullerene formation in flames (~5 ms).

The initial kinetic testing of the fullerene formation mechanism was performed using thermodynamic properties derived by a group additivity method for curved PAH and fullerenes[21]. In subsequent work[29], the group additivity method was found to have serious limitations in its ability to treat the energetics of curvature-induced ring strain and H-H repulsion, via comparison with MM3(92)[30] calculations for all the species in the fullerene formation mechanism and MOPAC calculations[31] (MNDO, AM1 and PM3; both RHF and UHF) for nine key species (fluoranthene, benzo[ghi]fluoranthene, corannulene, HB, TB, FB, XB, C_{60}, and C_{70}). All the calculated thermochemical properties[29] include evaluations of standard entropies and heat capacities. General conclusions[29] were: 1) MM3(92) best predicts the experimental heats of formation of C_{60} and C_{70}[32]; 2) MM3(92) also well predicts $C_p^\circ(g)$ of C_{60}[33] (within 6%) in the range 300 K $\leq$ T $\leq$ 500 K; 3) all the semi-empirical quantum mechanics methods used give similar values for ΔH_f° of the fullerene precursors on a relative basis, although differing greatly on an absolute basis; 4) the RHF ΔH_f° values for a given Hamiltonian are always larger than the corresponding UHF values, by as much as 16%; 5) a group additivity method for ΔH_f° of fullerenes[34] shows similar limitations to the previously developed group additivity method[21] in its ability to account for curvature-induced ring strain. It was also found that the predicted rates for C_{60} and C_{70} formation are minimally affected by use of the MM3(92) thermochemical properties as compared to the original work, showing that none of the reactions in the fullerene formation mechanism has an insuperable thermodynamic barrier[23]. This point will be proven below.

In the present work thermodynamic limitations for the formation of fullerenes C_{60} and C_{70} are addressed using the thermochemical properties previously calculated[29], along with experimental data for heats of formation of C_{60} and C_{70}[32]. First, we briefly revisit the McKinnon[35] global equilibrium calculations for C_{60}, both with and without C_{70}. Next, the entire reaction

sequence for the formation of C_{60} in the fullerene formation mechanism[22] is studied to look for thermodynamic bottlenecks in the form of disfavored reactions. A similar analysis[21] but using the group additivity properties shows the reactions leading up to the formation of HB to be disfavored, and as such, among the rate-limiting steps in the mechanism. Here, HB is shown to be the "top of the hill" in terms of its stability, and therefore the final section is devoted to a relative stability analysis of several $C_{30}H_x$ PAH (x=10,12,14,16,18; including two recently synthesized $C_{30}H_{12}$ compounds[36,37]). Formation of curved PAH is shown to be thermodynamically favored under certain conditions. Data from a fullerene-producing flame[12,28] are used in this portion of the analysis.

GLOBAL EQUILIBRIUM

A general assessment of thermodynamic driving forces in flame environments can be obtained from global equilibrium calculations. In this approach, a set of species and their thermodynamic properties are input, and the equilibrium concentrations of the entire mixture is computed for given conditions (input mole fractions, temperature, pressure). The software used is the version of STANJAN[38] compatible with the CHEMKIN-II subroutine packages[39]. STANJAN minimizes the free energy of the species set without need for a set of reactions as constraints. The present work differs from that of McKinnon[35] in the following ways: 1) properties for C_{60} and C_{70} use the experimental ΔH_f° values[32] with the MM3(92) values for S° and C_p°[29]; 2) only benzene flames are considered (therefore, the atomic C/H ratio is fixed at unity); and 3) the species set is expanded to include not only all the stable species in the fullerene formation mechanism[22], but also an extended series of PAH containing only 6-rings (PAH6) having the most peri-condensed (i.e., the most densely packed) structures up to and including D_{6h}-$C_{96}H_{24}$ (circumcircumcoronene -- A37 in Frenklach et al. nomenclature[40]). Large PAH are included to approximate the tendency to form soot. The set of 132 species used includes all 47 of the species used by McKinnon, with no changes in their thermochemical properties except for C_{60}.

One of the more important results from global equilibrium calculations in fuel-rich flames is that virtually no hydrocarbons are formed until the atomic C/O ratio exceeds unity, which is in sharp contrast to experimental observations. For example, in premixed benzene/oxygen flames many hydrocarbons including PAH are formed at C/O values much less than unity, and even soot begins to form at C/O = 0.76[41]. This discrepancy reflects the kinetic, not thermodynamic, control of carbonaceous species growth in flames. Therefore, global equilibrium calculations are not reliable quantitatively, but can yield useful insights into trends with respect to variables such as temperature and pressure.

The calculations below are for an input mixture of benzene and O_2 with C/O = 1.2, to allow sufficient production of hydrocarbons to study trends. The temperature is varied by 100 K intervals between 1000 and 3000 K, for four pressures which more than cover the range of known fullerene-producing

flames (20 Torr, 100 Torr, 1 atm, 10 atm). The oxygen input almost completely (>99.9%) appears as CO, (except for T < 1500 K and p ≥ 1 atm), and the hydrogen which does not appear as hydrocarbons is in the form of either H_2 or H atom. Approximately 5/6 of the carbon input appears as CO, leaving about 1/6 of the carbon available for hydrocarbons or fullerenes formation.

Equilibrium species concentrations are shown in Figs. 1-4. With increasing temperature, the available carbon appears first as CH_4, then as PAH (almost all of which is in the form of the largest PAH in the species set, A37), then fullerenes, and then $C_{2n}H_2$ (including C_2H_2, C_4H_2, C_6H_2, C_8H_2, with the overwhelming majority appearing as C_2H_2). The concentrations are expressed in terms of the fraction of carbon times 6, i.e. the fraction of available carbon, for a reaction set in which C_{60} is the only fullerene. At 20 Torr and 100 Torr, the peak amount of C_{60} contains over 90% of the available carbon. At 1 atm, the peak C_{60} concentration corresponds to a fraction of 77.1%, more than ten times the prediction of McKinnon[35] which was based on an earlier, now known to be overpredicted, value of ΔH_f° of C_{60}. Even at 10 atm, as much as 32% of the available carbon is predicted to be C_{60}, which, if such conversions could be realized in practice, might be of considerable practical interest. However, the actual prospects for fullerene formation at high pressure appear to be quite minimal, because soot formation is strongly enhanced by increasing pressure[22,23]. Other general trends found by McKinnon were reproduced: the sequence with respect to temperature of the significant carbon-containing species; an abrupt change (over a range of less than 100 K) from PAH to fullerenes with increasing temperature; and decreasing amounts of fullerene formed with increasing pressure. Use here of the experimental value of ΔH_f° shows that global equilibrium favors fullerene formation just about as much as it does any other carbonaceous product under the proper temperature and pressure conditions.

Using the experimentally measured ΔH_f° of C_{70}[32], another set of calculations in which C_{70} is also included was performed. The predictions for C_{70} and C_{60} are shown in Figures 5 and 6. Not surprisingly, C_{70} is predicted to be much more prevalent than C_{60}, effectively replacing it as compared to the case where C_{60} is the only fullerene. Also, the transition from PAH to fullerenes occurs at a slightly lower temperature (by ~100 K) for C_{70}, reflecting both the greater stability of C_{70}, and the slightly increased similarity of its molecular nature, due to its elongated structure, to planar PAH. However, a noticeable amount of C_{60} (peaking around 1.3-3.6% of the available carbon) is still predicted, far exceeding what a simple partial equilibrium prediction for the two fullerenes alone would yield[42,43]. The predicted molar C_{70}/C_{60} ratio of at least ~6 for 20 Torr and 100 Torr in the range of 1800-2500 K is still appreciably larger than typical experimental ratios of roughly 1.5 to 2[17,19,20,28], reinforcing the notion that fullerene formation is under kinetic control. Therefore thermodynamic barriers, which determine the ratio of the rate coefficients of the individual reactions in the forward and reverse directions, are of

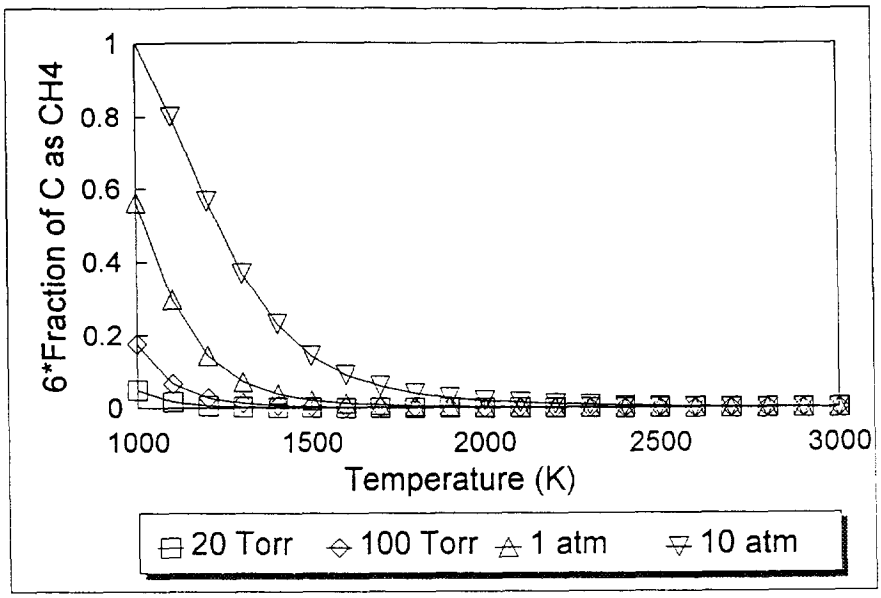

Figure 1. Global equilibrium predictions for CH_4 for C/O = 1.2, T = 1000-3000 K, selected pressures. (No C_{70} in species set.)

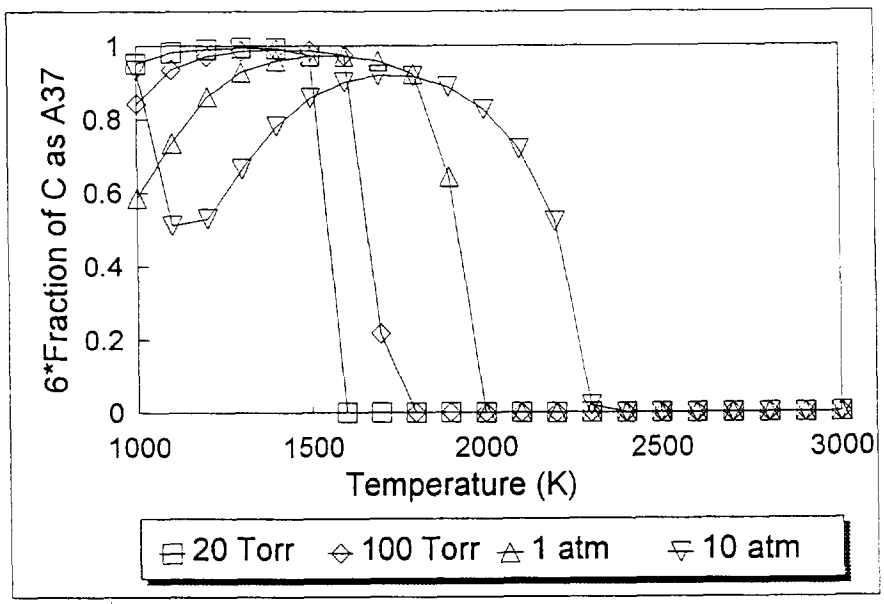

Figure 2. Global equilibrium predictions for A37 for C/O = 1.2, T = 1000-3000 K, selected pressures. (No C_{70} in species set.)

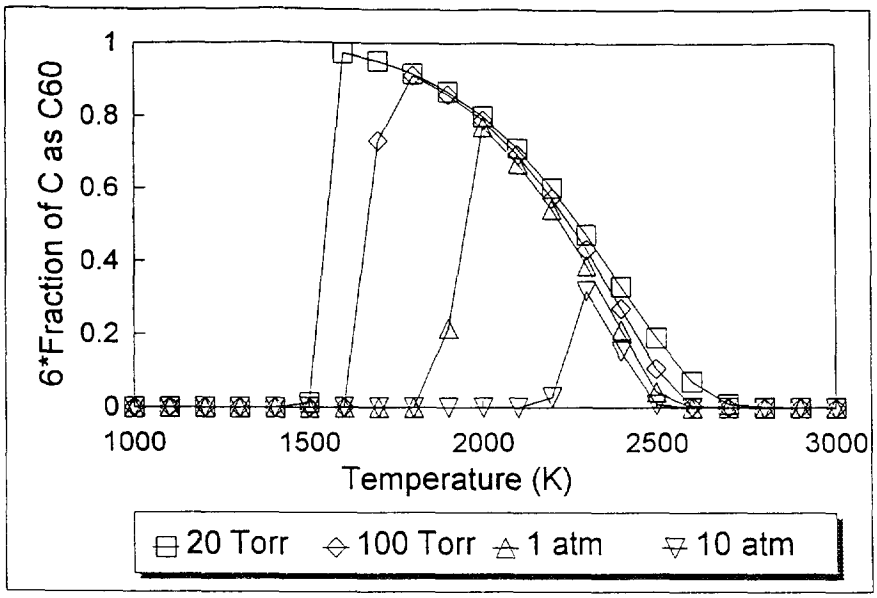

Figure 3. Global equilibrium predictions for C_{60} for C/O = 1.2, T = 1000-3000 K, selected pressures. (No C_{70} in species set.)

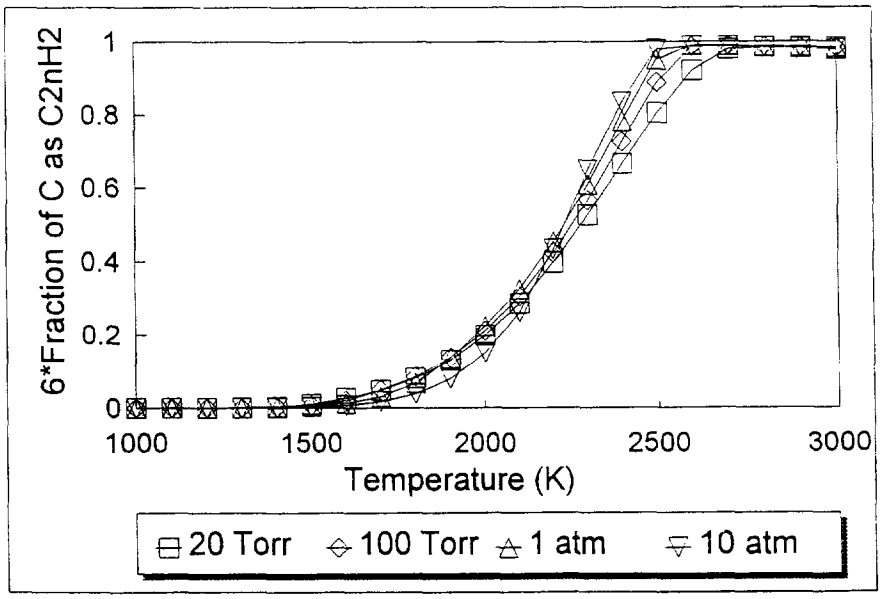

Figure 4. Global equilibrium predictions for $C_{2n}H_2$ for C/O = 1.2, T = 1000-3000 K, selected pressures. (No C_{70} in species set.)

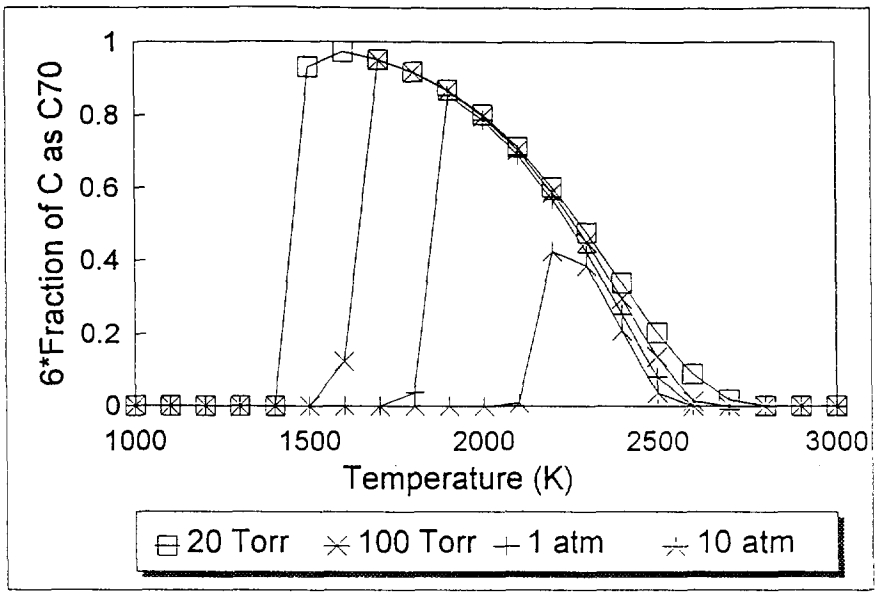

Figure 5. Global equilibrium predictions for C_{70} for C/O = 1.2, T = 1000-3000 K, selected pressures.

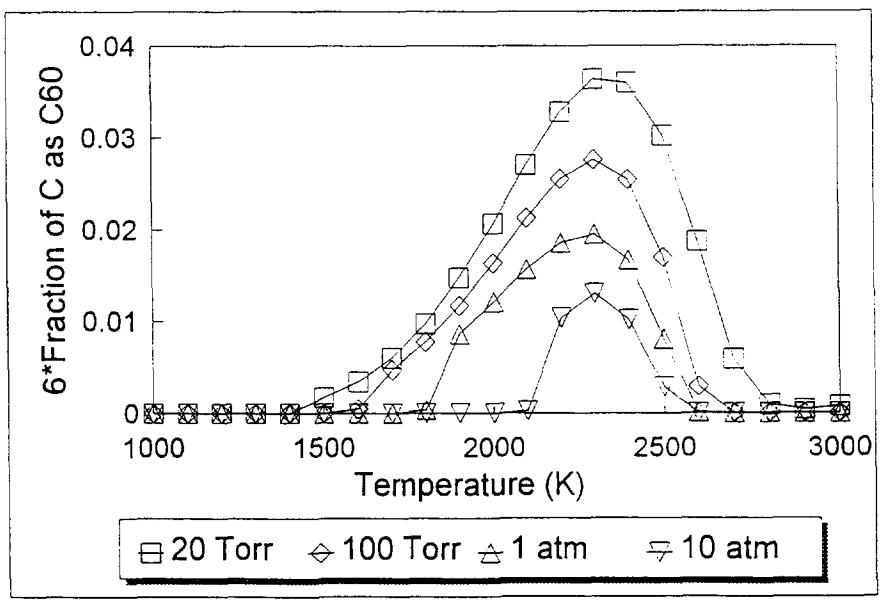

Figure 6. Global equilibrium predictions for C_{60} for C/O = 1.2, T = 1000-3000 K, selected pressures. (With C_{70} in species set.)

considerable interest in the fullerene formation mechanism[22].

C_{60} FORMATION -- STEP BY STEP

The shorthand nomenclature used for the stable species in the portion of the fullerene formation mechanism between fluoranthene and C_{60}, as well as the empirical formulae, are given in Table 1. Names for the corresponding sigma radicals formed by abstraction of an H atom are those for the stable compound followed by *, e.g. COR* ($C_{20}H_9$). Molecular structures for these compounds are given in reference 22, as well as the rationale for the nomenclature[44]. The species C_2H_2, H, and H_2 also appear in the mechanism.

Table 1. Names and Empirical Formulae for the Stable Species in the Portion of the Fullerene Formation Mechanism[22] Leading to C_{60} Formation.

	name	empirical formula		name	empirical formula		name	empirical formula
a)	FLTHN	$C_{16}H_{10}$	k)	HB3	$C_{36}H_{10}$	u)	FB2QR	$C_{54}H_{10}$
b)	BGHIF	$C_{18}H_{10}$	l)	HB4	$C_{38}H_{10}$	v)	FB2QRD	$C_{54}H_8$
c)	COR	$C_{20}H_{10}$	m)	TB	$C_{40}H_{10}$	w)	FB3Q	$C_{56}H_8$
d)	COR1	$C_{22}H_{10}$	n)	TB1	$C_{42}H_{10}$	x)	FB3QD	$C_{56}H_6$
e)	COR2	$C_{24}H_{10}$	o)	TB2	$C_{44}H_{10}$	y)	FB4Q	$C_{58}H_6$
f)	COR3	$C_{26}H_{10}$	p)	TB3	$C_{46}H_{10}$	z)	FB4QD	$C_{58}H_4$
g)	COR4	$C_{28}H_{10}$	q)	TB4	$C_{48}H_{10}$	aa)	FB5Q	$C_{60}H_4$
h)	HB	$C_{30}H_{10}$	r)	FB	$C_{50}H_{10}$	ab)	FB5QD	$C_{60}H_2$
i)	HB1	$C_{32}H_{10}$	s)	FB1	$C_{52}H_{10}$	ac)	C60	C_{60}
j)	HB2	$C_{34}H_{10}$	t)	FB2Q	$C_{54}H_{10}$			

The reactions in the fullerene formation mechanism[22] are listed in Table 2, along with the reaction type, ΔH_f°(298 K), ΔS°(298 K), ΔG(2050 K), and K_p'(2050 K) for each reaction. (K_p' is defined below.) The temperature 2050 K was chosen as a representative temperature for the fullerene-forming region of a premixed benzene/oxygen/10% argon flame operating at 40 Torr[12,28], which was used to provide data for the preliminary testing of the mechanism[22]. Mole fractions for H, H_2, and C_2H_2 were also taken as representative values for the same region of the flame, and were set at 0.025, 0.12, and 0.06, respectively. Rate coefficients for the four reaction types were taken from similar reactions for planar PAH. Sensitivities of the predicted fullerene formation rates to the input parameters have been previously published[22,23].

The overall reaction, FLTHN ($C_{16}H_{10}$) + 22 C_2H_2 = C_{60} + 27 H_2, is very strongly favored: ΔH_f°(298 K) = -664.4 kcal/mol, and ΔG(2050 K) = -416.1 kcal/mol. However, several of the individual reactions are thermodynamically disfavored. If only ΔH_f°(298 K) is considered, all the type 1 and 5-3 reactions would appear to be energetically uphill. However, at the temperatures of interest for fullerene formation, the effects of entropy must be considered. Reactions #4, 6, 8, 10, 12, 14, 16, 18, and 51 have ΔG(2050 K) > 0; all of these are type 23 reactions. Reaction 51, the last C_2H_2 addition, yields a $C_{60}H_4$ product with the hydrogen atoms so close to

Table 2. Reactions for Formation of C_{60} from Fluoranthene from the Fullerene Formation Mechanism[22], with Reaction Type, ΔH_f°(298 K), ΔS°(298 K), ΔG°(2050 K), and K_p'(2050 K). (See text for discussion.) Units are kcal/mol for ΔH_f° and ΔG°, and cal/mol-K for ΔS°. (K_p' is dimensionless.)

#	reaction	type	ΔH_f°(298 K)	ΔS°(298 K)	ΔG°(2050 K)	K_p'(2050 K)
1)	FLTHN + H = FLTHN* + H2	1	7.90	6.40	-4.15	5.77E-01
2)	FLTHN* + C2H2 = BGHIF + H	23	-38.80	-18.10	-4.78	7.76E+00
3)	BGHIF + H = BGHIF* + H2	1	7.90	5.00	-1.18	2.78E-01
4)	BGHIF* + C2H2 = COR + H	23	-36.60	-22.00	4.41	8.12E-01
5)	COR + H = COR* + H2	1	7.90	8.20	-7.80	1.41E+00
6)	COR* + C2H2 = COR1 + H	23	-26.20	-16.90	3.64	9.83E-01
7)	COR1 + H = COR1* + H2	1	5.90	5.10	-3.48	4.90E-01
8)	COR1* + C2H2 = COR2 + H	23	-27.90	-16.80	1.96	1.48E+00
9)	COR2 + H = COR2* + H2	1	6.00	5.00	-3.18	4.54E-01
10)	COR2* + C2H2 = COR3 + H	23	-28.50	-16.80	1.32	1.74E+00
11)	COR3 + H = COR3* + H2	1	5.90	5.00	-3.24	4.62E-01
12)	COR3* + C2H2 = COR4 + H	23	-29.30	-16.70	0.26	2.25E+00
13)	COR4 + H = COR4* + H2	1	6.00	5.00	-3.11	4.47E-01
14)	COR4* + C2H2 = HB + H	23	-33.40	-20.00	3.03	1.14E+00
15)	HB + H = HB* + H2	1	3.80	8.10	-13.39	5.58E+00
16)	HB* + C2H2 = HB1 + H	23	-34.10	-18.50	2.57	1.28E+00
17)	HB1 + H = HB1* + H2	1	3.80	4.90	-6.83	1.12E+00
18)	HB1* + C2H2 = HB2 + H	23	-35.90	-18.60	1.11	1.83E+00
19)	HB2 + H = HB2* + H2	1	3.80	4.90	-6.80	1.11E+00
20)	HB2* + C2H2 = HB3 + H	23	-39.70	-18.60	-2.61	4.55E+00
21)	HB3 + H = HB3* + H2	1	3.80	4.90	-6.83	1.11E+00
22)	HB3* + C2H2 = HB4 + H	23	-55.70	-19.00	-17.52	1.77E+02
23)	HB4 + H = HB4* + H2	1	3.80	4.90	-6.83	1.11E+00
24)	HB4* + C2H2 = TB + H	23	-56.90	-22.00	-12.51	5.18E+01
25)	TB + H = TB* + H2	1	8.00	8.20	-7.74	1.39E+00
26)	TB* + C2H2 = TB1 + H	23	-46.20	-19.00	-10.20	2.94E+01
27)	TB1 + H = TB1* + H2	1	6.00	5.10	-3.35	4.74E-01
28)	TB1* + C2H2 = TB2 + H	23	-46.00	-18.90	-10.11	2.87E+01

Table 2 (cont.). Reactions for Formation of C_{60} from Fluoranthene from the Fullerene Formation Mechanism[22], with Reaction Type, ΔH_f°(298 K), ΔS°(298 K), ΔG°(2050 K), and K_p'(2050 K). (See text for discussion.) Units are kcal/mol for ΔH_f° and ΔG°, and cal/mol-K for ΔS°. (K_p' is dimensionless.)

#	reaction	type	ΔH_f°(298 K)	ΔS°(298 K)	ΔG°(2050 K)	K_p'(2050 K)
29)	TB2 + H = TB2* + H2	1	5.90	5.00	-3.28	4.66E-01
30)	TB2* + C2H2 = TB3 + H	23	-46.10	-18.80	-10.49	3.15E+01
31)	TB3 + H = TB3* + H2	1	6.00	5.00	-3.18	4.55E-01
32)	TB3* + C2H2 = TB4 + H	23	-45.90	-18.90	-10.04	2.82E+01
33)	TB4 + H = TB4* + H2	1	5.90	5.10	-3.48	4.90E-01
34)	TB4* + C2H2 = FB + H	23	-47.10	-22.10	-4.52	7.28E+00
35)	FB + H = FB* + H2	1	8.00	8.30	-7.91	1.45E+00
36)	FB* + C2H2 = FB1 + H	23	-45.70	-18.70	-10.51	3.17E+01
37)	FB1 + H = FB1* + H2	1	5.90	5.00	-3.28	4.66E-01
38)	FB1* + C2H2 = FB2Q + H	23	-29.40	-15.70	-1.56	3.52E+00
39)	FB2Q = FB2QR	6	-0.40	0.10	-0.28	1.07E+00
40)	FB2QR + H = FB2QR* + H2	1	7.90	5.00	-1.28	2.85E-01
41)	FB2QR* = FB2QRD + H	5-3	11.60	19.30	-32.12	2.02E+06
42)	FB2QRD + H = FB2QRD* + H2	1	6.00	5.00	-3.08	4.44E-01
43)	FB2QRD* + C2H2 = FB3Q + H	23	-39.40	-17.10	-7.53	1.52E+01
44)	FB3Q + H = FB3Q* + H2	1	8.00	5.10	-1.42	2.95E-01
45)	FB3Q* = FB3QD + H	5-3	8.30	19.20	-34.64	3.75E+06
46)	FB3QD + H = FB3QD* + H2	1	5.90	5.00	-3.28	4.66E-01
47)	FB3QD* + C2H2 = FB4Q + H	23	-40.30	-18.70	-5.18	8.55E+00
48)	FB4Q + H = FB4Q* + H2	1	7.90	5.10	-1.45	2.98E-01
49)	FB4Q* = FB4QD + H	5-3	11.40	20.00	-33.52	2.85E+06
50)	FB4QD + H = FB4QD* + H2	1	6.00	6.40	-5.98	9.05E-01
51)	FB4QD* + C2H2 = FB5Q + H	23	-31.80	-19.10	3.82	9.39E-01
52)	FB5Q + H = FB5Q* + H2	1	5.90	5.10	-3.45	4.86E-01
53)	FB5Q* = FB5QD + H	5-3	18.20	27.70	-43.62	3.40E+07
54)	FB5QD + H = FB5QD* + H2	1	6.00	5.00	-3.14	4.51E-01
55)	FB5QD* = C60 + H	5-3	-43.80	9.40	-64.41	5.60E+09

each other that steric hindrance is important. All the other reactions for which $\Delta G(2050\ K) > 0$ are ring-forming reactions in which considerable amounts of curvature are introduced into the growing structure.

The entropy change for the reaction types helps to explain previously published predicted trends in fullerene formation rate with respect to temperature[23], in which the fullerene formation rate exhibits a maximum around 2100 K. While reactions of types 1 and 5-3 have $\Delta S^\circ > 0$, becoming more favored with increasing temperature, type 23 reactions have $\Delta S^\circ < 0$, showing the reverse temperature trend, while the type 6 reaction has $\Delta S^\circ \cong 0$.

The need to consider ΔG at the conditions of interest, instead of $\Delta H_f^\circ(298\ K)$ has been shown. However, the concentrations of the reactants themselves need to be included in the analysis to determine the relative ratio of forward to reverse reaction rates. During the kinetic testing previously performed, the mole fractions of H, H_2, and C_2H_2 remain effectively constant, varying by less than 0.5%[21], making all the reactions in the fullerene formation mechanism pseudo-first-order in both directions. While K_p (= exp[-ΔG/RT], where R is the ideal gas constant) is the ratio of the forward to the reverse rate for a given reaction, the relevant quantity for assessing the driving force for forward progress in the reaction becomes K_p', which is $K_p * p_H / p_{H2}$ for type 1 reactions, $K_p * p_{C2H2} / p_H$ for type 23 reactions, and K_p / p_H for type 5-3 reactions, where p_X is the partial pressure of reactant X. This approach is equivalent to using Legendre transforms of ΔG for the case where one or more species is at a constant chemical potential[45]. K_p' is not only the ratio of the pseudo-first-order forward to reverse rates, but also the equilibrium ratio of the fullerene precursor product to the reactant, e.g. [FLTHN*]/[FLTHN]. The equilibrium ratio for the overall reaction, $[C_{60}]/[FLTHN]$, is $5.5*10^{48}$.

Looking at K_p' for the individual reactions (Table 2) reveals yet another picture of thermodynamically hindered reactions in the mechanism. Of the 53 reactions, 22 (19 of type 1, 3 of type 23) have faster reverse reactions than forward reactions, i.e., $K_p' < 1$. However, a reverse rate need not be faster than the forward rate to have an impact on kinetic modeling results. Consideration of reactions in which the forward rate is less than three times faster than the reverse rate ($K_p' < 3$) can be more illustrative. Such reactions include all but one (#15) of the type 1 reactions, the nine type 23 reactions mentioned above for which $\Delta G(2050\ K) > 0$, and the type 6 reaction (#39).

The thermodynamic properties of the radical species relative to the corresponding stable species depend upon the type of aromatic carbon from which H-abstraction occurs[29,46]. Furthermore, the change in symmetry in forming the radical also affects the entropy change for reaction, and entropy is important at the temperature of interest. The combination of these two effects (more stable radical, loss of symmetry) makes reaction #15 the most favored of the type 1 reactions, but even so, the K_p' value is not very large (5.58). Therefore, the H-abstraction reactions are important for controlling the overall rate of curved PAH growth leading to fullerene

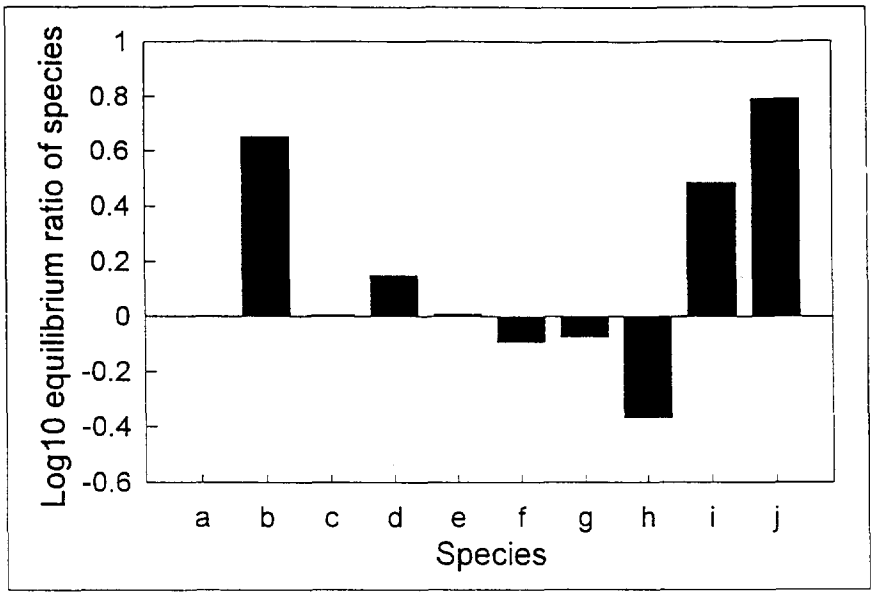

Figure 7. Log_{10} of the equilibrium ratio between the stable species in the fullerene formation mechanism with respect to species a (FLTHN) for species a-j.

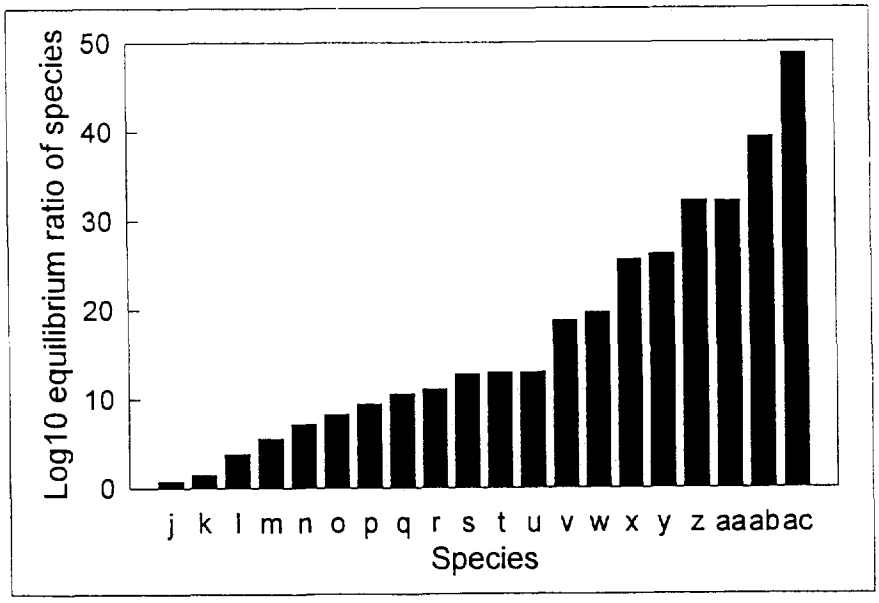

Figure 8. Log_{10} of the equilibrium ratio between the stable species in the fullerene formation mechanism with respect to species a (FLTHN) for species j-ac.

formation, with the molar H/H_2 ratio being a crucial reactor condition. This result is similar to that found in modeling planar PAH growth in flames[47].

Beyond the type 1 reactions, most of the thermodynamically hindered reactions (#4, 6, 8, 10, 12, 14, 16, 18) are found in the early stages of the mechanism, up to HB formation, with most of the remaining reactions being *de facto* irreversible reactions, with the exceptions occurring within the cage-closing portion leading to final C_{60} formation: the type 6 (intramolecular rearrangement) reaction is essentially thermoneutral (#39), and reaction #51 is discussed above. All the type 5-3 reactions are irreversible (with $K_p^{\cdot} > 2*10^6$), including the final reaction which forms the completed C_{60}, showing that opening of the C_{60} cage via H-atom attack is not a pathway for C_{60} destruction in flames.

A simple way of reviewing the overall driving forces in the mechanism is to plot the equilibrium concentration of the individual species with respect to FLTHN, which is merely the product of the $K_p^{\cdot}$ ratios of all the preceding reactions. The results are plotted in Fig. 7 for species a-j in Table 1 (FLTHN-HB2), and Fig. 8 for species j-ac (HB2-C_{60}). As asserted above, HB (species h) is indeed the least stable of the species in the mechanism, the thermodynamic "top of the hill". Additional ring formation beyond HB is very much thermodynamically favored, except for the reactions forming FB2QR (species u) and FB5Q (species aa), but by the time formation of the cage has proceeded this far, it is unlikely that these steps provide a real impediment to fullerene formation.

Of course, the equilibrium ratios shown in Figs. 7 and 8 are not seen in actuality. The fullerene formation mechanism is a simplified example of the most direct pathway to forming fullerenes C_{60} and C_{70} in flames. There are myriad other molecular weight growth products which are possible, most of which are unsuitable for further growth which will lead to a closed fullerene cage. Also, coagulations among PAH are very likely to produce species which do not have a suitable structure for eventual fullerene formation. Furthermore, the curved PAH can, like planar PAH, be consumed by coagulation with soot particles. It is not surprising then that, to date, while fluoranthene and benzo[ghi]fluoranthene have long been observed in flames[48,49], the existence of corannulene in flames has only recently been confirmed[50]. Except for C_{60} and C_{70} themselves, none of the species larger than corannulene in the mechanism has yet been positively identified. This lack of evidence begs the question of whether curved PAH such as HB can possibly form in flames.

RELATIVE STABILITY OF $C_{30}H_x$ SPECIES

The structures of six $C_{30}H_x$ compounds are shown below. The IUPAC names and empirical formulae are: **1** -- pentacyclopenta[*bc,ef,hi,kl,no*]corannulene, $C_{30}H_{10}$; **2** -- phenanthro[6,5,4,3-*ad*]corannulene, $C_{30}H_{12}$; **3** -- benz[5,6]-*as*-indaceno-[3,2,1,8,7-*mnopqr*]indeno[4,3,2,1-*cdef*]chrysene, $C_{30}H_{12}$; **4** -- dibenzo[*bc,ef*]coronene, $C_{30}H_{14}$; **5** -- tribenzo[*b,ghi,n*]perylene, $C_{30}H_{16}$; **6** -- heptaphene, $C_{30}H_{18}$. Species

1 is HB from the fullerene formation mechanism[22], **2**[36] and **3**[37] have recently been synthesized, and **4**, **5**, and **6** are planar PAH with the same point group as **2** (C_{2v})[51]. Compound **4** is also representative of the peri-condensed PAH6 preferentially formed in flames. The MM3(92) thermodynamic properties for these six molecules and literature values for H_2[52] are shown in Table 3.

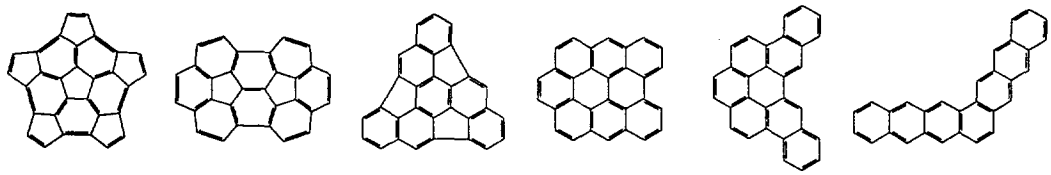

1 **2** **3** **4** **5** **6**

Table 3. MM3(92) Calculated Properties for **1-6** (**1**, reference 29; **2-6**, present work), and Literature Properties for H_2 (reference 52). Units are kcal/mol (ΔH_f°), and cal/mol-K (S°, C_p).

	ΔH_f°	S°	$C_p(300)$	$C_p(400)$	$C_p(500)$	$C_p(600)$	$C_p(800)$	$C_p(1000)$	$C_p(1500)$
1	277.33	130.33	86.30	112.24	133.37	150.10	173.80	189.18	209.86
2	198.85	131.39	85.98	112.65	134.72	152.49	178.17	195.18	218.42
3	213.55	134.32	86.63	113.39	135.48	153.20	178.74	195.61	218.64
4	112.27	135.97	86.95	114.54	137.66	156.41	183.77	202.07	227.39
5	110.91	145.59	90.86	119.24	143.10	162.48	190.89	210.07	236.90
6	124.58	151.99	94.63	124.06	148.76	168.81	198.29	218.32	246.60
H_2	0.00	31.21	6.90	6.96	7.00	7.02	7.07	7.21	7.73

The following overall reactions are considered, not to imply any chemical mechanisms, but to assess relative driving forces for curved PAH formation among the above $C_{30}H_x$ species: i) **6** = **5** + H_2, ii) **5** = **4** + H_2, iii) **4** = **2** + H_2, iv) **2** = **1** + H_2, v) **3** = **2**, vi) **4** = **1** + 2 H_2. The ΔG for these six reactions is shown for selected temperatures in Table 4. Reactions i and ii are very strongly favored, which is consistent with the long-observed prevalence of the most peri-condensed structures for flame PAH[53]; these two reactions will not be considered further. Reaction v gives the relative importance of the two $C_{30}H_{12}$ compounds recently synthesized[36,37]. Consistent with the analysis of Abdourazak et al.[37], which is based on MM2 values for ΔH_f°[54], **2** is more stable than **3**, dramatically so at lower temperatures: K_p for reaction v is 5.84 at 2050 K (and $5.7*10^5$ at 500 K).

The remainder of the analysis will center on reactions iii, iv, and vi (which is merely the sum of reactions iii and iv). Crossover temperatures (at which ΔG = 0) are 2932 K and 2265 K for reactions iii and iv, respectively. Since flames rarely reach such temperatures, it would appear that curved species could never become the predominant $C_{30}H_x$ compounds. Using the actual flame temperatures and H_2 partial pressures from the above-mentioned ϕ=2.2 benzene/oxygen flame[12], given in Table 5, the equilibrium ratios **2**/**4** (reaction iii), **1**/**2** (iv), and **1**/**4** (vi) are shown in Fig. 9.

Table 4. ΔG (kcal/mol) for Overall Reactions i-vi (see text for definition).

T(K)	i	ii	iii	iv	v	vi
500	-26.14	-9.64	72.99	63.01	-13.16	136.00
1000	-39.21	-21.18	57.88	45.41	-11.34	103.29
1500	-52.06	-32.58	42.58	27.34	-9.38	69.92
1750	-58.36	-38.16	35.02	18.34	-8.39	53.36
2000	-64.58	-43.66	27.51	9.40	-7.39	36.91
2250	-70.73	-49.09	20.06	0.52	-6.38	20.58
2500	-76.80	-54.44	12.66	-8.29	-5.38	4.37
2750	-82.81	-59.72	5.31	-17.02	-4.39	-11.71
3000	-88.75	-64.94	-1.98	-25.69	-3.39	-27.68

Table 5. Data from 40 Torr ϕ=2.2 benzene/oxygen flame. HAB stands for height above burner surface.

HAB (mm)	T(K)	p_{H2}(atm)
5	1999	0.00521
6	2070	0.00500
7	2105	0.00542
8	2118	0.00568
9	2120	0.00689
10	2122	0.00716
12	2108	0.00764
15	2088	0.00837

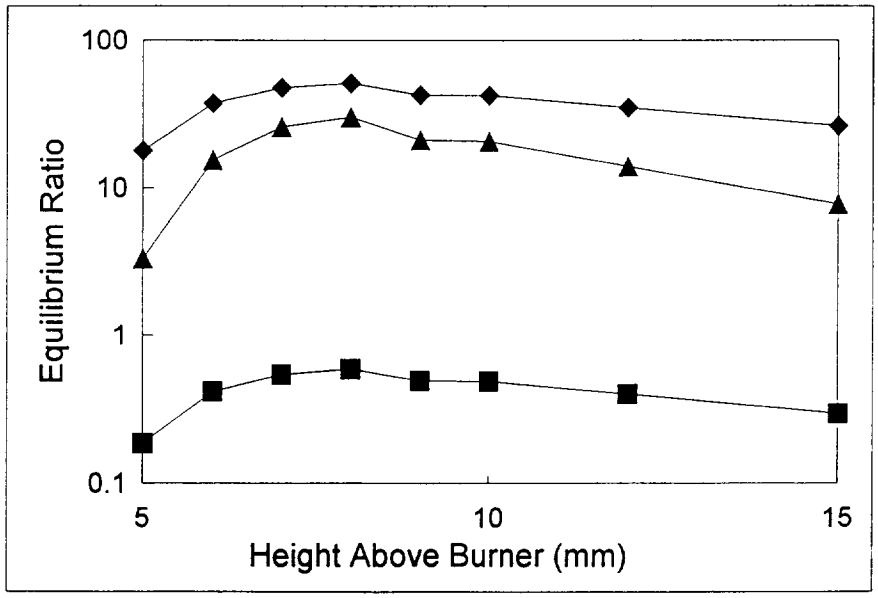

Figure 9. Equilibrium ratios for 2/4 (squares), 1/2 (diamonds), and 1/4 (triangles) in a benzene/oxygen flame.

While **4** is more stable than **2** under these conditions, **1** is more stable than either **2** or **4**. The compound with the highest ΔH_f° (**1**) has been found, paradoxically, to be the most stable[55]. Since **1** has the smallest possible number of hydrogen atoms for a $C_{30}H_x$ PAH containing only 5-rings and 6-rings without adjacent pentagons[24], there is indeed a strong driving force for curved PAH formation under these conditions. The results are strongly dependent upon p_{H2}. Considering the hypothetical case of the same flame at atmospheric pressure, the H_2 mole fraction does not vary strongly with pressure, so p_{H2} would be 19 times larger. In such a case, the **1**/**4** ratio has a maximum of only 0.083! In summary, conditions favoring curved PAH such as those in the fullerene formation mechanism as opposed to planar PAH are high temperatures and low partial pressures of H_2, the latter effectively translating to low overall pressure.

CONCLUSIONS

A consistent set of conditions has been found which would, according to thermodynamics, promote the formation of fullerenes and the curved PAH which are their proposed precursors. From global equilibrium considerations, lower pressures increase the potential peak amount of fullerenes possible, and also widen the temperature "window" for fullerenes formation. There are no insuperable thermodynamic barriers for fullerene formation for any of the reactions in the fullerene formation mechanism[22] considered here. Previous kinetic testing[23] has shown that the mechanism predicts a peak fullerene formation rate around 2100 K, consistent with the global equilibrium predictions. The most thermodynamically uphill portion of the mechanism is that leading up to HB formation. However, although HB is the least stable molecule in the mechanism, its formation relative to planar $C_{30}H_x$ species is favored at high enough temperatures (of order 2000 K) and low partial pressures of H_2. This understanding of thermodynamic constraints for fullerene formation can assist further study of the chemistry and kinetics of fullerene formation and the optimization of fullerene production in flames.

ACKNOWLEDGEMENTS

We are grateful to the Division of Chemical Sciences, Office of Basic Energy Sciences, Office of Energy Research, U.S. Department of Energy, for financial support under Grant Number DE-FG02-84ER13282, and to the MIT Center on Airborne Organics (EPA Grant to A.F. Sarofim) for financial support. The authors also thank Prof. J.T. McKinnon (Colorado School of Mines) for helpful support for the global equilibrium calculations, including species sets and thermodynamic properties.

REFERENCES AND NOTES

1. Zhang, Q.; O'Brien, S. C.; Heath, J. R.; Liu, Y.; Curl, R. F.; Kroto, H. W.; Smalley, R. E. *J. Phys. Chem.*, **1986**, *90*, 525.
2. Kroto, H. W.; McKay, K. *Nature*, **1988**, *331*, 328.
3. Curl, R. F.; Smalley, R.E. *Science*, **1988**, *242*, 1017.
4. Kroto, H. W. *Science*, **1988**, *242*, 1139.
5. Kroto, H. W.; Allaf, A. W.; Balm, S. P. *Chem. Rev.*, **1991**, *91*, 1213.
6. Kroto, H. W. *J. Chem. Soc. Faraday Trans.*, **1991**, *87*, 2871.
7. Kroto, H. W. *Angew. Chem. Int. Ed. Engl.*, **1992**, *31*, 111.
8. Gerhardt, Ph.; Löffler, S.; Homann, K.-H. *Chem. Phys. Lett.*, **1987**, 137, 306; *Twenty-Second Symposium (International) on Combustion*; The Combustion Institute: Pittsburgh, 1989; p. 395.
9. Löffler, S.; Homann, K.-H. *Twenty-Third Symposium (International) on Combustion*; The Combustion Institute: Pittsburgh, 1990; p. 355.
10. Howard, J. B.; Bittner, J. D. *Soot in Combustion Systems and its Toxic Properties*; Lahaye, J.; Prado, G.; Eds.; Plenum Press, New York, 1983.
11. Pope, C. J., M.S. Thesis, Massachusetts Institute of Technology 1988.
12. McKinnon, J. T., Ph.D. Thesis, Massachusetts Institute of Technology 1989.
13. Krätschmer, W.; Lamb, L. D.; Fostiropoulos, K.; Huffman, D. R. *Nature*, **1990**, *347*, 354.
14. Taylor, R.; Hare, J. P.; Abdul-Sada, A.K.; Kroto, H. W. *J. Chem. Soc., Chem. Commun.*, **1990**, 1423.
15. Ajie, H.; Alvarez, M. M.; Anz, S. J.; Bech, R. D.; Diederich, F.; Fositopoulos, K.; Huffman, D. R.; Krätschmer, W.; Rubin, Y.; Schriver, K. E.; Sensharma, D.; Whetten, R. L. *J. Phys. Chem.*, **1990**, *94*, 8630.
16. Haufler, R. E.; Conceicao, J.; Chibante, L. P. F.; Chai, Y.; Byrne, N. E.; Flanagan, S.; Haley, M. M.; O'Brien, S. C.; Pan, C.; Xiao, Z.; Billups, W. E.; Ciufolini, M. A.; Hauge, R. H.; Margrave, J. L.; Wilson, L. J.; Curl, R. F.; Smalley, R. E. *J. Phys. Chem.*, **1990**, *94*, 8634.
17. Howard, J. B.; McKinnon, J. T.; Makarovsky, Y.; Lafleur, A.; Johnson, M. E. *Nature*, **1991**, *352*, 139.
18. McKinnon, J. T.; Bell, W. L.; Barkley, R. B. *Combustion and Flame*, **1992**, *88*, 102.
19. Howard, J. B.; McKinnon, J. T.; Johnson, M. E.; Makarovsky, Y.; Lafleur, A. *J. Phys. Chem.*, **1992**, *96*, 6657.
20. Howard, J. B.; Lafleur, A. L.; Makarovsky, Y.; Mitra, S.; Pope, C. J.; Yadav, T. K. *Carbon*, **1992**, *30*, 1183.
21. Pope, C. J., Ph.D. Thesis, Massachusetts Institute of Technology 1993.
22. Pope, C. J.; Marr, J. A.; Howard, J. B. *J. Phys. Chem.*, **1993**, *97*, 11001.
23. Pope, C. J.; Howard, J. B. *Twenty-Fifth Symposium (International) on Combustion*; Combustion Institute: Pittsburgh, 1994; p. 671.
24. Smalley, R. E. *Acc. Chem. Res.*, **1992**, *25*, 92.
25. Scott, L. T.; Roelofs, N. H. *J. Am. Chem. Soc.*, **1987**, *109*, 5461.
26. Baum, Th.; Löffler, S.; Weilmünster, P.; Homann, K.-H. *ACS Div. Fuel Chem. Preprints*, **1991**, *36*, 1533.
27. Baum, Th.; Löffler, S.; Löffler, Ph.; Weilmünster, P.; Homann, K.-H. *Ber. Bunsenges. Phys. Chem.*, **1992**, *96*, 841.
28. Mitra, S.; Pope, C. J.; Gleason, K. K.; Makarovsky, Y.; Lafleur, A. L.; Howard, J. B. *Mat. Res. Soc. Symp. Proc.*, **1992**, *270*, 149.
29. Pope, C. J.; Howard, J. B. *J. Phys. Chem.*, **1995**, *99*, 4306.
30. Allinger, N. L.; Li, F.; Yan, L.; Tai, J. C. *J. Computational Chem.*, **1990**, *11*, 868.
31. Stewart, J. J. P. *QCPE*, **1986**, *18*, 455.
32. Beckhaus, H.-D.; Verevkin, S.; Rüchardt, C.; Diedrich, F.; Thilgen, C.; ter Meer, H.-U.; Mohn, H.; Müller, W. *Angew. Chem. Int. Ed. Engl.*, **1994**, *33*, 996.
33. Jin, Y.; Cheng, J.; Varma-Nair, M.; Liang, G.; Fu, Y.; Wunderlich, B.; Xiang, X.-D.; Mostovoy, R.; Zettl, A. K. *J. Phys. Chem.*, **1992**, *96*, 5151.
34. Armitage, D. A. 'Fred'; Bird, C.W. *Tetrahedron Lett.*, **1993**, *34*, 5811.
35. McKinnon, J. T., *J. Phys. Chem.*, **1991**, *95*, 8941.
36. Rabideau, P. W.; Abdourazak, A. H.; Folsom, H. E.; Marcinow, Z.; Sygula, A.; Sygula, R. *J. Am. Chem. Soc.*, **1994**, *116*, 7891.
37. Abdourazak, A. H.; Marcinow, Z.; Sygula, A.; Sygula, R.; Rabideau, P. W. *J. Am. Chem. Soc.*, **1995**, *117*, 6410.
38. Reynolds, W. C. *STANJAN Multicomponent Equilibrium Program* v.3.60, available on disk, 1986.
39. Kee, R. J.; Rupley, F. M.; Miller, J. A. *Chemkin-II: A Fortran Chemical Kinetics Package for the Analysis of Gas-Phase Chemical Kinetics*, Rep. SAND89-8009, Sandia National Laboratory, Livermore, CA, 1989.
40. Frenklach, M.; Clary, D. W.; Gardiner, W. C., Jr.; Stein, S. E. *Twentieth Symposium (International) on Combustion*; The Combustion Institute: Pittsburgh, 1984; p. 887.

41. Bittner, J. D.; Howard, J. B. *Eighteenth Symposium (International) on Combustion*; The Combustion Institute: Pittsburgh, 1981; p. 1105.
42. Slanina, Z.; Rudziński, J. M.; Ōsawa, E. *Carbon*, **1987**, *25*, 747.
43. Slanina, Z.; Rudziński, J. M.; Togasi, M.; Ōsawa, E. *Thermochim. Acta*, **1989**, *140*, 87.
44. Reference 22 is necessary background for fully understanding this section of the present work.
45. Alberty, R. A.; Oppenheim, I. *J. Chem. Phys.*, **1988**, *89*, 3689.
46. Chen, R. H.; Kafafi, S. A.; Stein, S. E. *J. Am. Chem. Soc.*, **1989**, *111*, 1418.
47. Frenklach, M.; Warnatz, J. *Comb. Sci. Tech.*, **1987**, *51*, 265.
48. Prado, G. P.; Lee, M. L.; Hites, R. A.; Hoult, D. P.; Howard, J. B. *Sixteenth Symposium (International) on Combustion*; The Combustion Institute: Pittsburgh, 1976; p. 649.
49. Chakraborty, B. B.; Long, R. *Environ. Sci. Tech.*, **1967**, *1*, 828.
50. Lafleur, A. L.; Howard, J. B.; Marr, J. A.; Yadav, T. *J. Phys. Chem.*, **1993**, *97*, 13539.
51. The synthesis of 2 was the motivation for this section of the present work. Accordingly, the planar PAH6 were chosen to have the same point group symmetry as 2, so the the effect of symmetry on entropy can be ignored.
52. Kee, R. J.; Rupley, F. M.; Miller, J. A. *The Chemkin Thermodynamic Data Base*, Rep. SAND87-8215B, Sandia National Laboratory, Livermore, CA, 1990.
53. Homann, K.-H. *Twentieth Symposium (International) on Combustion*; The Combustion Institute: Pittsburgh, 1984; p. 857.
54. The MM2 values calculated by Adbourazak et al. (reference 37) differ considerably from the MM3(92) values from the present work. Their calculated ΔH_f° values are (in kcal/mol) 264 (1), 182 (2), 198 (3).
55. Since 1 has a higher degree of symmetry (C_{5v}) than 2 or 4 (C_{2v}), reactions iv and vi have an additional entropy loss of R*ln(5/2) as compared to the reactions i, ii, iii, and v, making the apparent stability of 1 even more impressive.

(*Received* 20 *July* 1995)